Nanoscale chiral valley-photon interface through optical spin-orbit coupling

Su-Hyun Gong[1,2], Filippo Alpeggiani[1,2], Beniamino Sciacca[2], Erik C. Garnett[2], L. Kuipers[1,2,*]

[1]Kavli Institute of Nanoscience, Department of Quantum Nanoscience, Delft University of Technology, P.O. Box 5046, 2600 GA Delft, The Netherlands

[2]Center for Nanophotonics, AMOLF, Science Park 104 1098 XG Amsterdam, The Netherlands.

*Correspondence to: L.Kuipers@tudelft.nl

Abstract:

The emergence of two-dimensional transition metal chalcogenide materials has sparked an intense activity in valleytronics as their valley information can be encoded and detected with the spin angular momentum of light. We demonstrate the valley-dependent directional coupling of light using a plasmonic nanowire-WS_2 layers system. We show that the valley pseudospin in WS_2 couples to transverse optical spin of the same handedness with a directional coupling efficiency of 90±1 %. Our results provide a platform for controlling, detecting and processing valley and spin information with precise optical control at the nanoscale.

One Sentence Summary:

Valley-dependent directional emission is successfully demonstrated at room temperature through spin-orbit coupling with a plasmonic nanowire.

Valleytronics and nanophotonics provide powerful routes to address the heating problem in electronics by offering an alternative to information transport with the charge of electrons (*1, 2*). Valley pseudospin provides an additional degree of freedom to encode and process binary information in matter, analogous to the spin degree of freedom. The emergence of two-dimensional transition metal dichalcogenides (TMDs) layers provide a versatile materials platform for both optoelectronics (*3*) and valleytronics (*4-9*). These materials have direct bandgaps consisting of two (energy-degenerate) valleys at the corners of the Brillouin zone (labeled K and K'). The spin and valley information in TMDs can be optically addressed and detected using the spin angular momentum of light, due to their valley-dependent optical selection rule (*7, 8, 10-12*). However, the relatively short lifetimes (< 10 ps) of valley-polarized excitons limit logical processes and the spatial transport of valley information (*2*). While valley information is difficult to transport in realistic material systems, particularly at room temperature, photons are ideal information carriers due to the normally small light-matter interaction. Nanoscale coupling of valley pseudospin to photonic degrees of freedom is desirable for on-chip integrated valley devices.

The spin angular momentum as a degree of freedom of light at the nanoscale offers the ability to influence and exploit light-matter interactions. In highly confined light fields, transverse optical spin angular momentum (t-OSAM) results from the spin-orbit interaction of light (*13-25*). This t-OSAM provides a robust one-to-one relation between the handedness of optical spin and the propagation direction of a photonic mode−so called spin-momentum locking−due to their time reversal symmetry. The information of spin angular momentum can be directly transferred to the direction of light and vice versa. Recently, t-OSAM-dependent directional coupling of light with near-unity efficiency has been successfully demonstrated

experimentally using various photonic structures e.g., optical fibers (*13-15*), metal surfaces (*16-18*), metasurfaces (*26*), semiconductor waveguides (*20*, *21*), or microdisks (*22*).

We demonstrate a room-temperature chiral-coupling interface between the transverse optical spin of a plasmonic nanowire mode and the valley pseudospin of tungsten disulfide (WS_2), which provides robust valley-polarized directional emission. The resulting coupling between the photonic path and valley-spin in TMD materials and the metallic nature of the waveguide should enable applications in valley-chiral networks, valley-gates, and quantum photonic devices.

Our configuration for a chiral valley-photon interface (Fig. 1A) consists of a combination of a few layer TMD and a single silver nanowire. The evanescent fields of the plasmonic guided modes possess t-OSAM perpendicular to the TMD layers. The population of excitons in the two different valleys K and K' can be directly controlled by a circularly polarized excitation laser. The radiative decay of a valley-polarized exciton is associated with a circular transition dipole, which emits valley-dependent circularly polarized light. This circular transition dipole couples to the plasmonic eigenstate with the same handedness of its local transverse optical spin. Due to this chiral coupling between the circular nature of the emission dipole of the valley-polarized exciton and the local direction-locked transverse optical spin, emission from the different valleys couples to plasmonic modes propagating in opposite directions (Fig. 1B) when the transverse optical spin is maximal. To obtain a high degree of valley polarization, we exploit the high spin-valley coupling strength and spin-layer locking effect of WS_2 (*27*, *28*). The degree of valley polarization is denoted by $P_V = (I_K - I_{K'})/(I_K + I_{K'})$, where I_K and $I_{K'}$ represent the photoluminescence (PL) intensity from K and K', respectively. The number of WS_2 layers is identified through their optical contrast in a microscope image and their PL spectrum (Fig. S1).

The results presented here are based on a WS_2 flake consisting of five layers. Its polarization-resolved spectrum, measured in the absence of the silver nanowire (Fig. 1C), reveals a measured $P_V = 0.7$ at room temperature. Figure 1D depicts an optical microscopy image of one of the samples and a collected photoluminescence image mostly from the indirect bandgap. The two bright spots at each end of the waveguide demonstrate that emission is coupled to the guided modes of the plasmonic nanowire. Through the chiral coupling, the valley information is converted to the propagation direction of the mode to which the exciton coupled: the plasmonic mode itself has no overall optical spin (Fig. S2). Under local excitation at the center of the silver nanowire, directional emission from the TMD layers is investigated by measuring light scattered at the ends of the wire.

To quantify the magnitude of the t-OSAM near a silver nanowire, we performed numerical calculations with a finite difference eigenmode (FDE) solver (Fig. 2A). The guided plasmonic mode exhibits strong evanescent fields at the glass-nanowire interface, i.e., exactly at the position of WS_2 layers. Due to the strong transverse confinement and the plasmonic nature of the modes, a large longitudinal (x-direction) component of the electric field is present. The *x* and *y* component of the electric field have comparable amplitudes and are roughly ±90 degrees out of phase: the modes exhibit a large t-OSAM. The local sign of the local t-OSAM has a one-to-one relation with the propagation direction of light and the position with respect to the mirror plane of the geometry (y-direction). We calculated the density of the t-OSAM as a function of position in the *x*-*y* plane, which corresponds to the Stokes parameter $S_3 = -2\,\mathrm{Im}(E_x E_y^*) / (E_x^2 + E_y^2)$ (*20*) (Fig 2B). The plasmonic guided modes of infinite length nanowires locally have a t-OSAM density near unity. The sign of the transverse optical spin on either side of the nanowire is opposite as expected from symmetry considerations. Clearly, when the propagation direction of

the mode is reversed, so are all the signs of the helicity everywhere. These results are qualitatively summarized in Fig. 2C that demonstrate that the handedness of optical spin is determined by a combination of *y* position and propagation direction.

We simulate the emission from one valley in WS_2 near a finite-length plasmonic nanowire with the three-dimensional finite-difference time-domain (FDTD) method. The polarized valley emission is described with a circular dipole. Figure 2D depicts the position-dependent directionality (D_0) of the emission of a left-handed circular dipole in the *x*-*y* plane. It is calculated from the light transmitted (T_L and T_R) to the left and right ends of the wire, $D_0(x,y) = (T_L(x,y) - T_R(x,y))/(T_L(x,y) + T_R(x,y))$. The first thing to note is that the circular dipole emission is preferentially coupled to a propagating mode with appropriate sign of optical spin (compare Figs. 2B, C). The second thing to notice is that a high degree of directionality is obtained, which is opposite in sign when exciting on either side of the nanowire. A standing-wave-like pattern is visible along the wire caused by a small reflection at the end of the finite length nanowire (7 μm) wire. Please note that the high value of directionality of 0.91 is still observed despite the presence of the low-amplitude counter-propagating mode which tends to reduce the t-OSAM and the directionality (*20*). To properly describe the experiment, merely calculating the directionality is insufficient: actual coupling of the emission to the guided modes is also required, Figure 2E depicts the normalized, position-dependent coupling strength, $\kappa_{tot}(x,y) = (T_L(x,y) + T_R(x,y))/(T_L(x,y) + T_R(x,y))_{\max}$. Combining D_0 and κ_{tot} results in the chiral coupling coefficient $\kappa_{\text{valley-path}}$ that describes how well emission from a specific valley couples to a one single direction of the light path: $\kappa_{valley-path}(x,y) = D_0(x,y) \cdot \kappa_{tot}(x,y)$. The calculated $\kappa_{\text{valley-path}}$ (Fig. 2F) shows that the experimentally obtained directionality will be dominated by emitting dipoles located close to the nanowire.

Far-field microscopy is used to verify the chiral valley-photon interface formed by directional coupling of WS_2 excitons to plasmonic nanowires. Valley-polarized excitons are locally excited at the middle of the silver nanowire (x=0) for different y-positions with a close-to diffraction-limited focal spot of a suitably polarized 594 nm laser. Note that the free-space focused laser light cannot couple to the plasmonic guided mode due to momentum mismatch (Fig. S3). An optical bandpass filter (620-630 nm) is used to predominantly collect the exciton emission for each excitation position. Raw data is presented in Figures 3A and 3B for right- and left-handed circular excitation polarization, respectively. The large central spot in each image is caused by exciton emission not coupled to the plasmonic nanowire. Comparing the images in Fig. 3A and 3B to Fig. 1D it is clear that the intensity of the spots at the end of the wire have a lower intensity relative to the central excitation spot. This decrease is caused by the fact that Fig. 1D is dominated by the emission from the indirect transition in the near infrared where the propagation losses are significantly less than at 620-630 nm where the direct exciton emission occurs (Fig. S3A). In the line traces the emission coupled to the nanowire shows up as clear peaks (shoulders) on top of a background caused by the excitation spot. Already in this raw data, the valley-controlled directional emission is visible to the "naked eye": for a given combination of handedness and excitation position, an asymmetry is obvious in the intensity of the spots at either end of the nanowire. The asymmetry of emission is reversed when either the excitation spot is moved to the other side of the nanowire or the polarization handedness of the excitation is flipped.

The PL intensity scattered at the left and right nanowire ends is used to quantify the valley-dependent directionality as a function of y. The extracted $I_L(y)$ and $I_R(y)$, the peak intensities after subtracting the background arising mainly form the excitation spot, reflect the

amount of exciton emission that is coupled to the left- and right-propagating plasmonic modes, respectively (see Fig. S4 for our subtracting method). The dotted curves in Fig. 3C and 3D denote the total guided PL intensity ($I_L(y) + I_R(y)$) as a function of the excitation position. They indicate that the excitons only couple to plasmonic modes when |y| < ~500 nm. We then determine the experimental directional coupling efficiency κ_{exp}:

$\kappa_{\exp}(y) = (I_L(y) - I_R(y))/(I_L(y) + I_R(y))$ (Fig. 3C, 3D). We observe a clear directional coupling: for left-handed excitation and centered above (y<0) and below (y>0) the nanowire, the exciton emission couples to plasmonic eigenstates propagating from right to left and left to right, respectively. When the handedness of the excitation is flipped so do the propagation directions of the plasmonic modes. The measurements display exactly the trends observed in the calculations. For symmetric excitation, i.e., excitation on the symmetry axis of the system at the center of the nanowire κ_{exp} is zero, as expected. A small offset in directionality, caused by a small displacement of the excitation spot with respect to the middle of the nanowire in combination with propagation losses, was subtracted from the measured result (Fig. S5). A more quantitative description and comparison with calculations will be presented below. The measurements have been reproduced for a number of plasmonic nanowires and WS_2 flakes with different layer thicknesses (Fig. S6). In all cases, a strong directionality was observed.

Measurements performed for different excitation polarizations and emission wavelengths confirm that the directional emission is caused by valley-dependent chiral coupling to the plasmonic modes. The direction in the CCD camera image of the luminescence perpendicular to the length of the nanowire is dispersed in wavelength using a grating. This configuration provides position-dependent PL spectra along the wire from which we can determine κ_{exp} for different wavelengths (Fig. 4). Figure 4C demonstrates that an equal mix of K and K' excitons,

generated by using a linear polarized excitation light, displays no directionality, while for the same nanowire K or K' excitons separately (Figures 4A, B) display valley-controlled directionality. Note that the maximum κ_{exp} in Fig. 4A and 4B (~0.17) are lower than the value we observed in Fig. 3 of 0.35. This is caused by the decreased signal to noise ratio, resulting from the fact that the wavelength dispersed image could, by its very nature, not resolve any spatial information along the *y*-direction (Fig. S7). Figures 4D-F show that the indirect bandgap emission, which does not exhibit valley polarization, does not display any directionality, regardless of position or excitation polarization. Together these results demonstrate that all experimentally observed directionality is attributable to valley-controlled chiral coupling to plasmonic modes.

Comparison of the experimental and the calculated results reveal two differences. First, the experimental directionality profile is spatially smeared out. Secondly, the magnitude of κ_{exp} is less than maximum in the calculations. In part this is caused by obvious experimental limitations, e.g. a finite excitation spot size and background noise: both decrease the experimental maximum of the directionality and the finite excitation spot size also spatially smears out the pattern. However, the reduction in directionality is also caused by the finite P_V of the WS_2 system itself. The valley-to-valley hopping (*29*) would actually flip the direction in which the plasmonic modes are launched. Therefore, the effective directionality with a finite P_V, would be a simple product of $\kappa_{\text{valley-path}}$ and P_V. These experimental matters are readily taken into account to properly compare our realized chiral valley-photon interface to the ideal simulated interface:

$$\kappa_{fit}(y) = \frac{[\kappa_{valley-path} \cdot P_V] \otimes PSF}{[\kappa_{tot} + 2\rho] \otimes PSF},$$

where $\kappa_{valley-path}$ is the calculated chiral valley-path coupling coefficient for perfect circularly polarized dipole, P_V is the measured degree of valley polarization (0.7), and ρ is an unpolarized background noise relative to the maximum signal and represents a heuristic decrease of chiral coupling. To account for the effect of the finite size of the excitation region, we convolute the calculated signal with the point spread function (PSF) estimated from the experimental data (Fig. S8, S9). We obtain excellent agreement between fit and data for ρ =0.009±0.005 (gray lines in Fig. 3C, D). With a reduction of directionality as $D_0/(1+2\rho/\kappa_{tot})$ the fitting procedure reveals that the experimental valley-to-path coupling efficiency including background noise is as high as 0.90±0.01. The quality of the fit yields a number of important conclusions. First, because the experimentally determined point spread function is sufficient to explain the broadening of the directional coupling efficiency, exciton diffusion does not significantly affect the experiment. Second, any effect of the plasmonic nanowire on the polarization of the excitation focal spot is negligible. Lastly and most importantly, the chiral valley-to-path coupling is only limited by the magnitude of the transverse optical spin of the plasmonic nanowire modes. Thus, we have been able to realize a room temperature interface between the valley pseudospin of WS_2 and the propagation direction of nanowire plasmonic modes with a fidelity as high as 0.9.

Our results show that the efficient coupling of valley-polarized excitons in WS_2 to the transverse optical spin of plasmonic nanowire modes result in valley-photon direction locking with high fidelity. The high valley-spin coupling strength of WS_2 and high transverse optical spin density in plasmonic modes provides a chiral valley (spin)-photon interface at room temperature and without the necessity of external magnetic fields. It is important to note that due to the one-to-one relation between optical path and the local transverse optical spin, the propagation direction of the guided light can also be exploited to transfer the valley degree of

freedom to other valley devices on a chip through suitable, localized breaking of mirror symmetry again exploiting the transverse optical spin of the mode, but now to excite. Realization of such an interface presents a platform for both fundamental studies and wide range of exciting applications of chiral photonics and chiral quantum optics.

References and Notes:

1. D. Xiao, W. Yao, Q. Niu, Valley-contrasting physics in graphene: magnetic moment and topological transport. *Phys. Rev. Lett.* **99**, 236809 (2007).
2. J. R. Schaibley, H. Yu, G. Clark, P. Rivera, J. S. Ross, K. L. Seyler, W. Yao, X. Xu, Valleytronics in 2D materials. *Nat. Rev. Mat.* **1**, 16055 (2016).
3. K. F. Mak, J. Shan, Photonics and optoelectronics of 2D semiconductor transition metal dichalcogenides. *Nat. Photon.* **10**, 216-226 (2016).
4. Q. H. Wang, K. Kalantar-Zadeh, A. Kis, J. N. Coleman, M. S. Strano, Electronics and optoelectronics of two-dimensional transition metal dichalcogenides. *Nat. Nanotechnol.* **7**, 699-712 (2012).
5. K. F. Mak, K. L. McGill, J. Park, P. L. McEuen, The valley Hall effect in MoS2 transistors. *Science* **344**, 1489-1492 (2014).
6. Y. Zhang, T. Oka, R. Suzuki, J. Ye, Y. Iwasa, Electrically switchable chiral light-emitting transistor. *Science* **344**, 725-728 (2014).
7. A. M. Jones, H. Yu, N. J. Ghimire, S. Wu, G. Aivazian, J. S. Ross, B. Zhao, J. Yan, D. G. Mandrus, D. Xiao, W. Yao, X. Xu, Optical generation of excitonic valley coherence in monolayer WSe2. *Nat. Nanotechnol.* **8**, 634-638 (2013).

8. X. Xu, W. Yao, D. Xiao, T. F. Heinz, Spin and pseudospins in layered transition metal dichalcogenides. *Nat. Phy.* **10**, 343-350 (2014).

9. D. Xiao, G.-B. Liu, W. Feng, X. Xu, W. Yao, Coupled spin and valley physics in monolayers of MoS 2 and other group-VI dichalcogenides. *Phys. Rev. Lett.* **108**, 196802 (2012).

10. H. Zeng, J. Dai, W. Yao, D. Xiao, X. Cui, Valley polarization in MoS2 monolayers by optical pumping. *Nat. Nanotechnol.* **7**, 490-493 (2012).

11. K. F. Mak, K. He, J. Shan, T. F. Heinz, Control of valley polarization in monolayer MoS2 by optical helicity. *Nat. Nanotechnol.* **7**, 494-498 (2012).

12. T. Cao, G. Wang, W. Han, H. Ye, C. Zhu, J. Shi, Q. Niu, P. Tan, E. Wang, B. Liu, J. Feng, Valley-selective circular dichroism of monolayer molybdenum disulphide. *Nat. Commun.* **3**, 887 (2012).

13. J. Petersen, J. Volz, A. Rauschenbeutel, Chiral nanophotonic waveguide interface based on spin-orbit interaction of light. *Science* **346**, 67-71 (2014).

14. C. Sayrin, C. Junge, R. Mitsch, B. Albrecht, D. O'Shea, P. Schneeweiss, J. Volz, A. Rauschenbeutel, Nanophotonic optical isolator controlled by the internal state of cold atoms. *Phys. Rev. X* **5**, 041036 (2015).

15. R. Mitsch, C. Sayrin, B. Albrecht, P. Schneeweiss, A. Rauschenbeutel, Quantum state-controlled directional spontaneous emission of photons into a nanophotonic waveguide. *Nat. Commun.* **5**, 5713 (2014).

16. F. J. Rodríguez-Fortuño, G. Marino, P. Ginzburg, D. O'Connor, A. Martínez, G. A. Wurtz, A. V. Zayats, Near-field interference for the unidirectional excitation of electromagnetic guided modes. *Science* **340**, 328-330 (2013).

17. D. O'Connor, P. Ginzburg, F. Rodríguez-Fortuño, G. Wurtz, A. Zayats, Spin–orbit coupling in surface plasmon scattering by nanostructures. *Nat. Commun.* **5**, 5327 (2014).

18. K. Y. Bliokh, D. Smirnova, F. Nori, Quantum spin Hall effect of light. *Science* **348**, 1448-1451 (2015).

19. K. Bliokh, F. Rodríguez-Fortuño, F. Nori, A. V. Zayats, Spin-orbit interactions of light. *Nat. Photon.* **9**, 796-808 (2015).

20. R. Coles, D. Price, J. Dixon, B. Royall, E. Clarke, P. Kok, M. Skolnick, A. Fox, M. Makhonin, Chirality of nanophotonic waveguide with embedded quantum emitter for unidirectional spin transfer. *Nat. Commun.* **7**, 11183 (2016).

21. B. Le Feber, N. Rotenberg, L. Kuipers, Nanophotonic control of circular dipole emission. *Nat. Commun.* **6**, 7695 (2015).

22. F. J. Rodríguez-Fortuño, I. Barber-Sanz, D. Puerto, A. Griol, A. Martínez, Resolving light handedness with an on-chip silicon microdisk. *ACS Photonics* **1**, 762-767 (2014).

23. K. Y. Bliokh, A. Y. Bekshaev, F. Nori, Extraordinary momentum and spin in evanescent waves. *Nat. Commun.* **5**, 3300 (2014).

24. A. Aiello, P. Banzer, M. Neugebauer, G. Leuchs, From transverse angular momentum to photonic wheels. *Nat. Photon.* **9**, 789-795 (2015).

25. T. Van Mechelen, Z. Jacob, Universal spin-momentum locking of evanescent waves. *Optica* **3**, 118-126 (2016).

26. T. Chervy, S. Azzini, E. Lorchat, S. Wang, Y. Gorodetski, J. A. Hutchison, S. Berciaud, T. W. Ebbesen, C. Genet, Spin-momentum locked polariton transport in the chiral strong coupling regime. *arXiv preprint arXiv:1701.07972*, (2017).

27. B. Zhu, H. Zeng, J. Dai, Z. Gong, X. Cui, Anomalously robust valley polarization and valley coherence in bilayer WS2. *Proc. Natl. Acd. Sci. U.S.A.* **111**, 11606-11611 (2014).

28. A. M. Jones, H. Yu, J. S. Ross, P. Klement, N. J. Ghimire, J. Yan, D. G. Mandrus, W. Yao, X. Xu, Spin-layer locking effects in optical orientation of exciton spin in bilayer WSe2. *Nat. Phy.* **10**, 130-134 (2014).

29. R. Schmidt, G. Berghäuser, R. Schneider, M. Selig, P. Tonndorf, E. Malić, A. Knorr, S. Michaelis de Vasconcellos, R. Bratschitsch, Ultrafast coulomb-induced intervalley coupling in atomically thin WS2. *Nat. Lett.* **16**, 2945-2950 (2016).

30. B. Sciacca, S. A. Mann, F. D. Tichelaar, H. W. Zandbergen, M. A. Van Huis, E. C. Garnett, Solution-phase epitaxial growth of quasi-monocrystalline cuprous oxide on metal nanowires. Nat. Lett. 14, 5891-5898 (2014).

31. W. Zhao, Z. Ghorannevis, L. Chu, M. Toh, C. Kloc, P.-H. Tan, G. Eda, Evolution of electronic structure in atomically thin sheets of WS2 and WSe2. ACS nano 7, 791-797 (2012).

32. B. Zhu, H. Zeng, J. Dai, Z. Gong, X. Cui, Anomalously robust valley polarization and valley coherence in bilayer WS2. Proc. Natl. Acd. Sci. U.S.A. 111, 11606-11611 (2014).

33. P. K. Nayak, F.-C. Lin, C.-H. Yeh, J.-S. Huang, P.-W. Chiu, Robust room temperature valley polarization in monolayer and bilayer WS2. Nanoscale 8, 6035-6042 (2016).

34. A. M. Jones, H. Yu, J. S. Ross, P. Klement, N. J. Ghimire, J. Yan, D. G. Mandrus, W. Yao, X. Xu, Spin-layer locking effects in optical orientation of exciton spin in bilayer WSe2. Nat. Phys. 10, 130-134 (2014).

35. H. S. Lee, M. S. Kim, Y. Jin, G. H. Han, Y. H. Lee, J. Kim, Efficient Exciton–Plasmon Conversion in Ag Nanowire/Monolayer MoS2 Hybrids: Direct Imaging and Quantitative

Estimation of Plasmon Coupling and Propagation. Advanced Optical Materials 3, 943-947 (2015).

36. Z. Zhu, J. Yuan, H. Zhou, J. Hu, J. Zhang, C. Wei, F. Yu, S. Chen, Y. Lan, Y. Yang, Excitonic resonant emission–absorption of surface plasmons in transition metal dichalcogenides for chip-level electronic–photonic integrated circuits. ACS Photonics 3, 869-874 (2016).

37. K. M. Goodfellow, R. Beams, C. Chakraborty, L. Novotny, A. N. Vamivakas, Integrated nanophotonics based on nanowire plasmons and atomically thin material. Optica 1, 149-152 (2014).

Acknowledgments: S.-H. G, F. A. and L. K acknowledge funding from ERC Advanced, Investigator Grant No. 340438-CONSTANS. This work is part of the research program of The Netherlands Organization for Scientific Research (NWO). F. A. acknowledges support from the Marie Skłodowska-Curie individual fellowship BISTRO-LIGHT (No. 748950). B.S. and E.C.G. were supported by funding from the European Research Council under the European Union's Seventh Framework Programme ((FP/2007-2013)/ERC grant agreement no. 337328, "Nano-EnabledPV". All data are reported in the main text and supplementary materials.

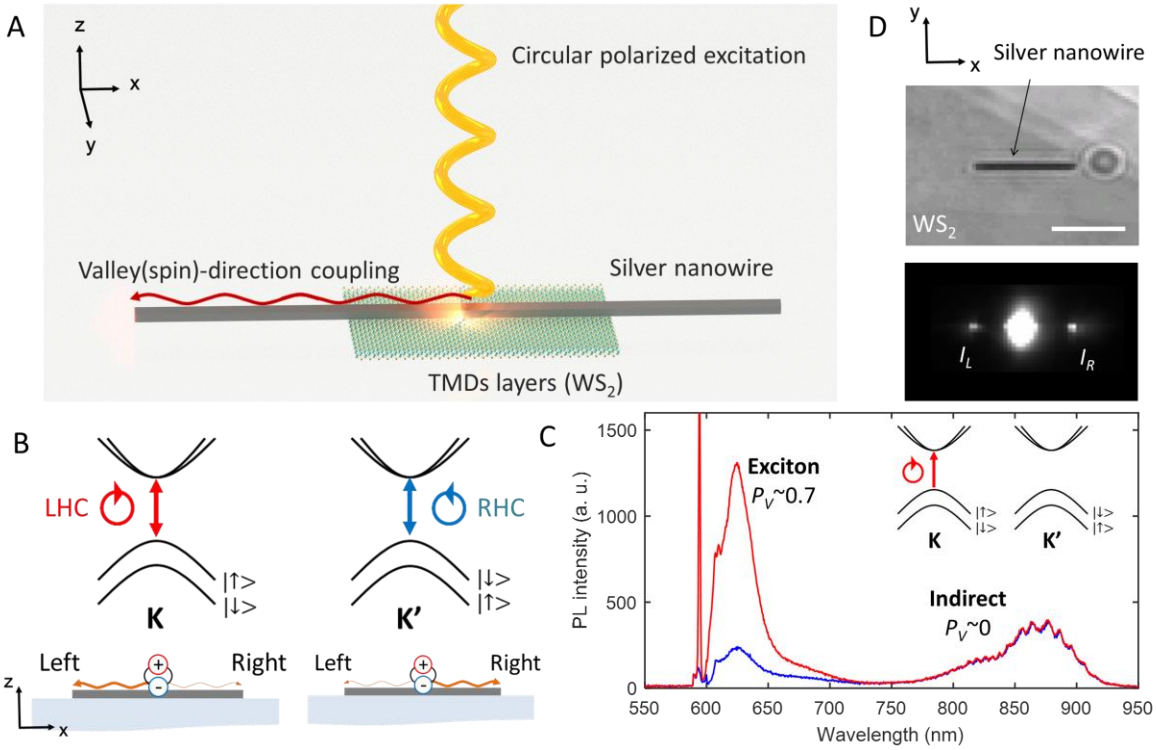

Fig. 1. Valley-controlled directional coupling of light (A) A conceptual illustration of directional emission of a valley-polarized exciton in WS_2. The valley pseudospin and photon-path are coupled by means of spin-orbit coupling of light. (B) A schematic sketch of the band diagram of WS_2 and its optical selection rules depending on the valley index. The two opposite-handed circularly polazired emissions from each valley would couple preferentially to mode propagating in opposite directions. (C) Polarization-resolved emission spectrum of WS_2, measured without a silver nanowire, at room temperature excited by a left-handed circularly polarized laser beam at 594 nm. Red and blue spectra indicate left and right handed circularly polarized emission, respectively. (D) Image of a fabricated WS_2-silver nanowire coupled system (top). WS_2 emission coupled to the plasmonic waveguide mode and scattered at the ends of the nanowire (bottom). The scale bar indicates 5 μm.

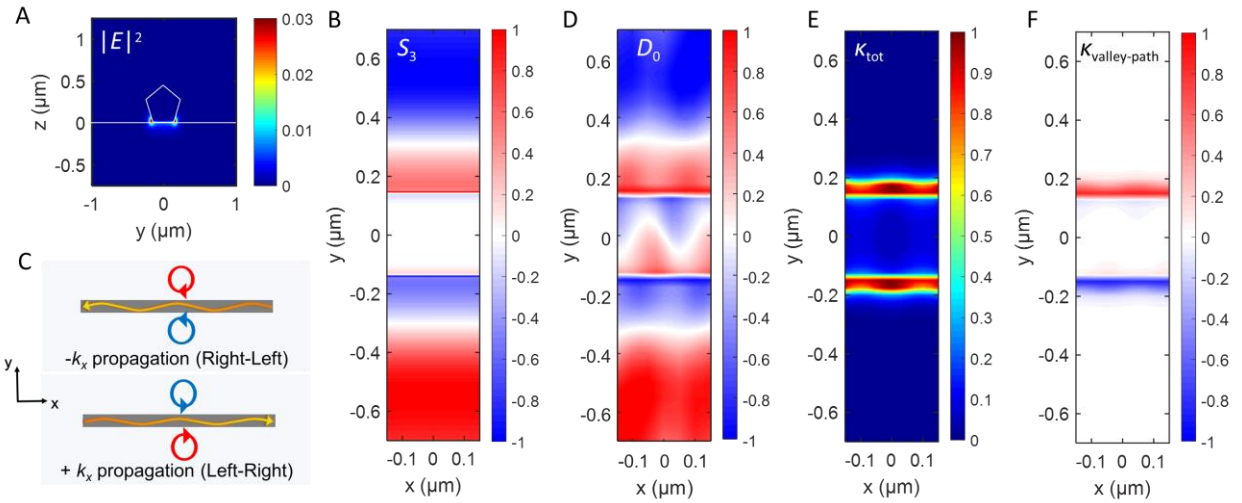

Fig. 2 Numerical modeling of the transverse spin angular momentum of light (A) Cross-sectional electric field distribution of the plasmonic guided mode. (B) Density of transverse optical spin, i.e. Stokes parameters S_3, of the in-plane (*x*-*y* plane) electric field component. (C) Illustration of the distribution of handedness of elliptical polarization, optical spin, which is depending on both the position and propagation direction. (D) Directionality of circularly polarized dipole emission, $D_0(x,y)$, as a function of its position. (E) Normalized coupling strength of circularly polarized dipole source to the plasmonic guided modes, $\kappa_{tot}(x,y)$ (F) Chiral coupling coefficient indicating how efficient circular dipole in one valley couples to a one direction of the guided mode, $\kappa_{valley-path}(x,y) = D_0(x,y) \cdot \kappa_{tot}(x,y)$.

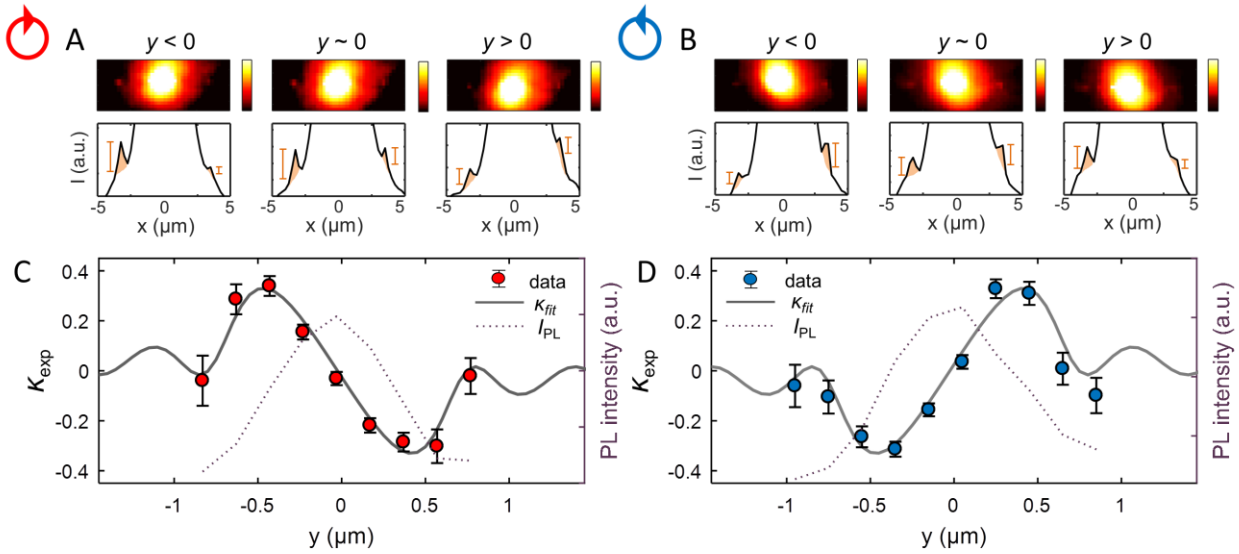

Fig. 3 Experimental demonstration of valley-controlled directional emission. (A and B) Fluorescence images of the emission of valley-polarized excitons (log scale; top) and line cuts of the intensity profiles (linear scale; bottom) along the silver nanowire under left- (A) and right- (B) handed circularly polarized-excitation. The intensities at the excitation regions were deliberately saturated for clarity of the images. The length of the silver nanowire is ~7 μm. (C and D) Measured directional coupling efficiency, $(I_L - I_R)/(I_L + I_R)$, of the guided emission as a function of the position of the excitation laser with the left- (C) and right- (D) handed circular polarization. Gray lines represent fitting results using the calculated directional coupling efficiency. Purple dotted lines correspond to the total PL intensity measured from the ends of the nanowire as a function of the excitation position.

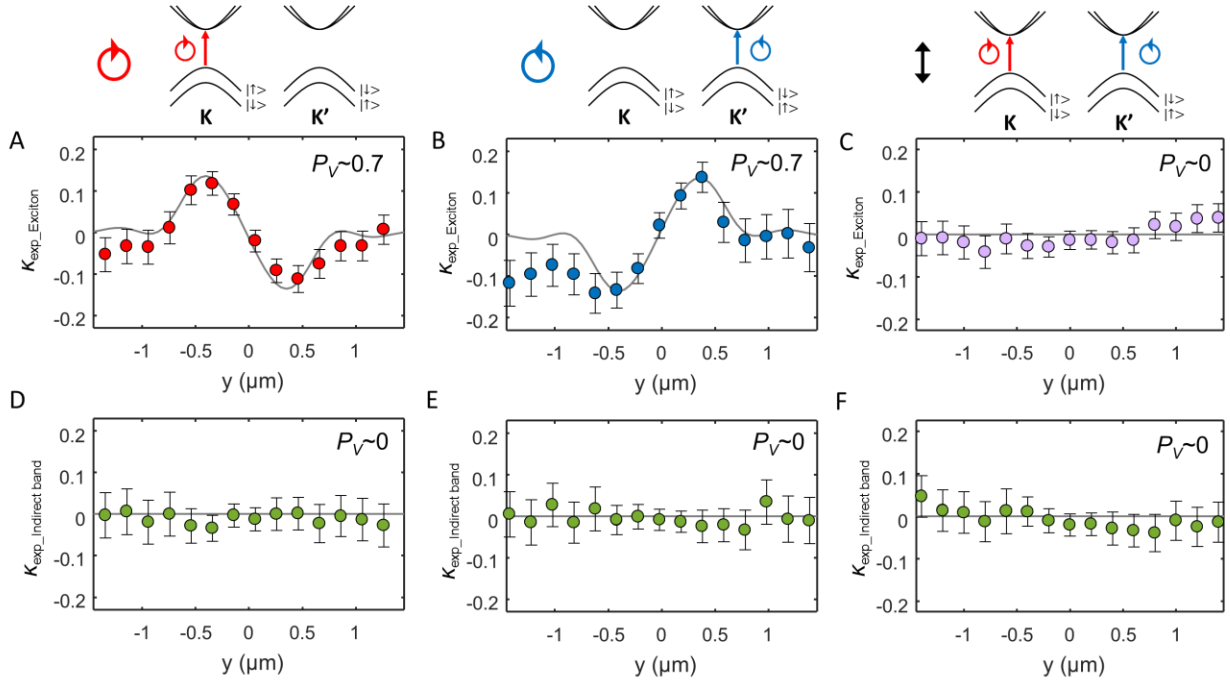

Fig. 4 Direct observation of directional emission induced by valley-path coupling of the valley-polarized exciton. The emission from the valley-polarized excitons shows directional emission which depends on both the position of excitation and the handedness of the circularly polarized laser (A, B), while the transition of the indirect bandgap has a non-directionality for both handednesses of the circularly polarized laser (D, E). A linearly polarized laser excitation leads to zero valley polarization so that both the exciton- (C) and indirect band- (F) transition exhibit no directionality. P_V indicates the degree of valley polarization, $P_V = (I_K - I_{K'})/(I_K + I_{K'})$.